Title
Cellular adaptations in vestibular epithelia of the Egyptian fruit bat

Author
Choy, Kristel Rae Wing Yee

Publication Date
2016

Peer reviewed|Thesis/dissertation

UNIVERSITY OF CALIFORNIA

Los Angeles

Cellular adaptations in vestibular epithelia of the Egyptian fruit bat

A thesis submitted in partial satisfaction of the requirements for the degree Master of Science in Physiological Science

by

Kristel Rae Wing Yee Choy

2016

ABSTRACT OF THE THESIS

Cellular adaptations in vestibular epithelia

of the Egyptian fruit bat

by

Kristel Rae Wing Yee Choy

Master of Science in Physiological Sciences

University of California, Los Angeles, 2016

Professor Walter Helmut Metzner, Co-Chair

Professor Larry F. Hoffman, Co-Chair

Bats are highly agile animals by virtue of their flight and echolocation behaviors, and they are acknowledged to be “spatiotemporal integration specialists.” In order to avoid obstacles, scavenge food, and capture prey, bats must be able to navigate a three-dimensional space. In flight, bats must perform high speed navigation through obstacles using a blend of sensory modalities including vision and echolocation. While some bat species exhibit structural adaptations to their cochleae as an adaptation to the demands of echolocation, there is an absence architectural adaptation of the vestibular labyrinth that would accommodate the increased demands for high frequency head movement coding associated with agile movement. The

present study tested the hypothesis that there may exist cellular adaptations within the vestibular epithelia consistent with increased capability for high fidelity head movement coding. This was accomplished using immunohistochemical analyses focusing primarily in the striolae of the utricles of *Rousettus aegyptiacus* and Mus *musculus,* regions bounded by the presence of calretinin (Calb2) positive calyces. Hair cell counts revealed increased proportions of type I hair cells (hair cells surrounded by calyces) in *Rousettus* when compared to *Mus* (72.6% ± 3.5% and 57.2% ± 2.7%, respectively, $p<10^{-5}$). Additionally, *Rousettus* exhibits increases in the proportion of complex calyces in the striola when compared to *Mus*. Ocm, a calcium binding protein expressed in vestibular hair cells, is also observed to have expanded expression in *Rousettus* and *Mus* both in the striola as well as the extrastriolar regions. These novel findings indicate that vestibular epithelia of *Rousettus* exhibit cellular adaptations over *Mus* that are consistent with increases in head movement coding capability associated with agile movement in flight.

The thesis of Kristel Rae Wing Yee Choy is approved.

Peter M. Narins

Felix Erich Schweizer

Walter Helmut Metzner, Committee Co-Chair

Larry F. Hoffman, Committee Co-Chair

University of California, Los Angeles

2016

TABLE OF CONTENTS

LIST OF TABLES AND FIGURES

ACKNOWLEDGMENTS

Thank you to my very patient mentors and committee members for all of their input and guidance, and thank you to my family and fiancé for all of their support during this endeavor.

INTRODUCTION

It is one of the main principles of neurobiology that the encoding of sensory information may change based on specific animal behaviors (Lettvin et al., 1959; Ulanovsky and Moss, 2008). The sensory system must adapt in order to successfully meet the requirements created by niche behaviors. Some behaviors, such as hunting may result in adaptations such as an enhanced sense of smell for bird dogs (Steen et al., 1996) or enhanced vision in raptors (Potier et al., 02016). In order to avoid obstacles, find food, and capture prey bats must be able to navigate a three-dimensional space. In flight, bats must perform high speed navigation through obstacles using a blend of sensory modalities including vision and echolocation. Research suggests that the vestibular system plays a role in orientation and flight control, integrating with both vision and echolocation to coordinate motion during complex flight (Horowitz et al., 2004).

Bats are highly agile animals by virtue of their flight and echolocation behaviors, and they are acknowledged to be “spatiotemporal integration specialists” (Ulanovsky and Moss, 2008). *Rousettus aegyptiacus*, the bat model used in this study, has been shown to have wing beat frequencies between 6-8 Hz (Riskin et al., 2010). Given the anti-phase movement of the bat body relative to wings in flight, this is indicative of similar frequencies *Rousettus'* body movement. In contrast to the agility seen in *Rousettus*, *Mus musculus*, the terrestrial animal model used in this study, has been seen to have lowered rotational sensitivity of afferents projecting from the cristae at >4 Hz head rotation (Lasker et al., 2008) which is consistent with earlier findings that mouse vestibular nuclei neurons show low sensitivity to head velocity and eye position when compared to rabbit, cat, and monkey (Beraneck and Cullen, 2007). Beraneck and Cullen (2007) suggest that these lower sensitivities may be due to the mouse having a “lower inertial load”, being less dependent on gaze stabilization, or simply having lower need. In

contrast, it may be expected that the blend of echolocation and visual behaviors required to properly navigate in flight may incur the need for enhanced vestibular function in bats.

It has been hypothesized that these flight and echolocation behaviors would benefit from enhanced capability for head movement coding of the vestibular system, as such input from the vestibular system would be integral in stabilizing both visual and auditory gaze during agile movement. Previous investigations have sought to identify adaptations within the architecture of the labyrinth associated with agility. While some bats exhibit enlarged cochleae as an adaptation for echolocation, there is an absence of structural adaptation of the bony labyrinth in bats, in comparison to other rodents, that would result in enhanced capability of the vestibular system for head movement coding (Ramprashad et al., 1980; Davies et al., 2013). Ramprashad et al. explored the possibility that *Myotis lucifugus* may exhibit increases in semicircular canal diameter thereby increasing the load placed on the cupula for a given head movement. Ramprashad et al. found no evidence for any biomechanical signal amplification in the vestibular architecture, a finding later confirmed by Davies et al. using CT scans across a wide range of bat species. The possibility that bats may exhibit cellular adaptations within the vestibular epithelia has yet to be explored, and if such adaptations exist, it is possible that they may enhance head movement coding capability proving beneficial to the bats unique behavioral repertoire.

In the utricle, the striola is associated with the vestibular afferents of greatest sensitivity (Goldberg et al., 1990). These regions are bounded by the presence of calretinin (Calb2) expressing calyces which are associated with a subtype of type I hair cell: type I_c. In addition to type I_c hair cells, hair cells associated with non-calretinin expressing calyces (type I_d) and hair cells not associated with a calyx (type II) are present within the striola. Additionally, all type I hair cells can be identified by using β-3-tubulin (β3T), a neuronal tubulin, to label all calyces

surrounding the type I hair cells. This increased ability for high fidelity head movement coding make the striola of specific interest in the exploration of cellular adaptation. These cellular adaptations within the vestibular epithelia may possibly be identified through varied expression and distribution of the markers oncomodulin (Ocm, aka β-parvalbumin) and KCNQ4. Ocm is a calcium binding protein expressed in vestibular and cochlear hair cells, and in utricles Ocm expression is closely associated with the striolar and peristriolar regions (Simmons et al., 2010; Hoffman et al.). Previous studies have shown that the potassium channel gene coding for KCNQ4, a low-voltage activated potassium channel, exhibits parallel evolution in echolating bats, ostensibly enhancing the capabilities for high frequency hearing (Liu et al., 2012). This channel has been found to be expressed in afferent calyces (Lysakowski et al., 2011; Spitzmaul et al., 2013). It is possible that in *Rousettus*, there may be an expansion of Ocm and KCNQ4 expression in comparison to *Mus.*

Additionally, the specific morphology of calyceal afferent endings may also play a role in the response characteristics of calyceal afferents. Complex calyces receiving input from more than one hair cell of the same polarity may exhibit increases in sensitivity to head movement, possibly serving as a mode of signal amplification over the simple calyces that receive input from only one hair cell (Fernandez et al., 1990). In pigeons, another animal that exhibits agile movement in the form of flight, the mean value of hair cells per calyx terminal has been observed to be >4 with the most complex calyces containing 9 hair cells (Si et al., 2003). Increased incidence of complex calyces over simple calyces within the striolar region point to another possible adaptation in *Rousettus* over *Mus*.

The findings of this current study provides novel evidence that *Rousettus aegyptiacus* exhibits morphological and cellular adaptations of the vestibular system.

METHODS

Dissection

All procedures were approved by the Chancellor's Animal Research Committee. Dissection of the vestibular epithelia from *Rousettus aegyptiacus* and *Mus musculus* proceeded as follows. The animals were deeply anesthetized using an intraperitoneal injection of sodium pentobarbital (5mg/kg, *Rousettus)* or exposure to isoflurane (*Mus*). After decapitation, the vestibular epithelia were initially exposed to 4% paraformaldehyde (PFA) in 0.1M phosphate buffered saline (PBS) either through the oval window (*Rousettus*) or through a fenestra created in the caudomedial temporal bone (*Mus*). The tissue was further exposed to PFA by debriding the floor of subarcuate fossa with a number 11 scalpel. The temporal bones were then quickly excised and immersed in the PFA solution overnight (*Rousettus*) or for 3 hours (*Mus*). After fixation, the vestibular epithelia were removed from the temporal bones intact by using fine forceps. Once removed, the epithelia were separated and the nerves were closely trimmed.

Antigen retrieval

Tissues that were to be labeled using KCNQ4 antibodies required an additional antigen retrieval step. Intact epithelia (whole-mount), stored in 0.1M PBS in 96-well plates, were treated with 10 mM citric acid (pH 6) by replacing the PBS in the well. The wells were then covered and the specimens were heated in the microwave for 15 minutes at 10% power. The specimens were allowed to cool for 2-5 minutes before being washed with PBS 3 times for 10 minutes. The specimens were then treated with the normal immunohistochemical procedures.

Immunohistochemistry

Immunohistochemical procedures were performed on whole-mount specimens. The specimens were first incubated in blocking solution (for Ocm labeled specimen: 1% Triton-X100, 10% fish gelatin blocking agent, in 0.1M PBS; for KCNQ4 labeled specimens: 1% Triton-X100, 2.5% normal goat serum, in 0.1M PBS) for 2 hours at room temperature. The specimens were then incubated in a cocktail of primary antibodies in blocking solution for 48-72 hours at 4°C. After incubation in the primary antibody cocktail, the tissues were washed 3 times for 10 minutes in 0.1M PBS. The specimens were then incubated in a cocktail of secondaries and stains in 0.1M PBS for 2 hours at room temperature. Concentrations of specific antibody cocktails are listed in Table 1.

Table 1

***Mus* Specimen with Ocm**							
1° Ab	**Conc.**	**Manufacturer**	**Product #**	**2° Ab/Stains**	**Conc.**	**Manufacturer**	**Product #**
Ms x Calb2	1:250	Millipore	MAB1568	Dk x Ms AF405	1:250	Abcam	ab175658
Rb x β3T	1:250	Biolegend	PRB-435P	Dk x Rb AF488	1:250	Life Technologies	A21206
Gt x Ocm	1:250	SCBT	sc-7446	Dk x Gt AF555	1:250	Life Technologies	A11056
				Phalloidin AF633	1:100	Molecular Probes	A22284
***Rousettus* Specimen with Ocm**							
1° Ab	**Conc.**	**Manufacturer**	**Product #**	**2° Ab/Stains**	**Conc.**	**Manufacturer**	**Product #**
Ms x Calb2	1:250	Millipore	MAB1568	Dk x Ms AF488	1:250	Life Technologies	A21202
Rb x β3T	1:250	Biolegend	PRB-435P	Dk x Rb AF647	1:250	Life Technologies	A31573
Gt x Ocm	1:250	SCBT	sc-7446	Dk x Gt AF555	1:250	Life Technologies	A11056
				Cytopainter iF405	1:100	Abcam	ab176752
				Alt: Phalloidin CF405	1:100	Biotium	00034
***Mus* Specimen with KCNQ4**							
1° Ab	**Conc.**	**Manufacturer**	**Product #**	**2° Ab/Stains**	**Conc.**	**Manufacturer**	**Product #**
Ms x KCNQ4	1:100	Neuromab	P56696	Gt x Ms 488	1:250	Life Technologies	A11001
Rb x Calb2	1:100	Millipore	ab5054	Gt x Rb 546	1:250	Life Technologies	A11010
				NucBlue (DAPI)	1:100	ThermoFisher	R37606
				Phalloidin AF633	1:100	Molecular Probes	A22284
***Rousettus* Specimen with KCNQ4**							
1° Ab	**Conc.**	**Manufacturer**	**Product #**	**2° Ab/Stains**	**Conc.**	**Manufacturer**	**Product #**
Ms x Calb2	1:250	Millipore	MAB1568	Gt x Ms 488	1:250	Life Technologies	A11001
Rb x KCNQ4	1:100	Neuromab	sc-50417	Gt x Rb 546	1:250	Life Technologies	A11010
				NucBlue (DAPI)	1:100	ThermoFisher	R37606
				Phalloidin AF633	1:100	Molecular Probes	A22284

Confocal microscopy

After immunohistochemical processing, the epithelia were mounted on Superfrost Plus Microscope Slides (12-550-15, Fisher Scientific) with a Secure-Seal Spacer (9 mm diameter, 0.12 mm deep, S24737, Fisher Scientific). Tissue was immersed in EverBrite mounting medium (23001, Biotium) and covered with number 1.5 coverslips (18x18 mm, 12-541A, Fisher). Tissues were then imaged using an upright LSM 710 confocal microscope using the Zeiss Zen 2012 software. The 405 nm (1-5% intensity), 488nm (5-15% intensity), 543nm (25-50% intensity), and 633 nm (8-12% intensity) laser lines were used for excitation. Low-power stacks were taken under a Zeiss Plan-Neofluar 10X/0.3 NA objective and high-power stacks were taken under a Zeiss Plan-Apochromat 63X/1.4 NA oil-immersion objective. For high power stacks the pinhole size for image acquisition was 49 µm for 2-channel line scans with 488 nm and 633 nm excitation and 42 µm for 2-channel line scans with 405 nm and 546 nm excitation. High-power stacks were taken through-out the striolar region, while the medial extrastriolar region was sampled. The optical section thickness was 0.37 µm and a sufficient number of optical sections were collected in order to image through the support cell layer. The total number of optical sections was dependent on the flatness of the tissue mounted on the slide. Overlapping stacks were taken throughout the entirety of the striola and additionally in the medial extrastriola. Images were acquired at 0.8x zoom in *Rousettus* and 1x zoom in *Mus* and overall x-y size was 1024 x 1024 pixels or 168.52 µm x 168.52 µm in *Rousettus* and 1500 x 1500 pixels or 134.86 µm x 134.86 µm in *Mus*. Average intensity projections were prepared using FIJI image analysis software. Because of the differences in zoom, the *Rousettus* images were cropped in order to create appropriate and comparable images in figures with both *Rousettus* and *Mus* tissues. Scale bars were placed by calculating µm/ pixel ratios. *Mus* images were also sized down to match the

cropped pixel sizes of *Rousettus* images.

Image analysis

Hair cell counts were completed using *Neurolucida* (version 6.02.2) on three *Rousettus* utricles from different animals. Hair cell counts from *Mus* as used in the present study were obtained from Hoffman et al. First, individual channels were separated from multi-channel high-power stacks to created single channel stacks that were then uploaded into *Neurolucida*. These stacks (i.e. from a single channel) were then stitched together to visualize the entire striola in each channel. Using the stacks with the channel representative of Calb2 labeling, all hair cells associated with Calb2-positive calyces were then identified and labeled with a marker. Then using the stacks with the channel representative of phalloidin (phal) staining, the area that demarcated the striola was identified by tracing along the tight junctions of the most peripheral hair cells associated with Calb2 positive calyces. Once the entire striolar region was traced, individual hair cells in the striola were marked and counted by identifying the base of stereocilia (visibly stained with phal) and the kinocilium void (not stained with phal) giving a total count of striolar hair cells. Using the channel representative of β3T labeling, all hair cells within the striola associated with calyces were marked and counted giving the total number of striolar type I hair cells. The total number of striolar type II hair cells was deduced by subtracting the total number of striolar type I hair cells from the total number of striolar hair cells.

In order to obtain counts of hair cells expressing Ocm, it was necessary to determine a minimum level of intensity as which hair cells were to be considered Ocm positive. Once minimum levels of intensity were determined, it allowed us to give each hair cell one of six different phenotypes: type Ic Ocm+, type Id Ocm+, type II Ocm+, type Ic Ocm-, type Id Ocm-,

and type II Ocm-. Using FIJI, mean intensity measurements were taken in hair cells at their widest point using a uniform region of interest circle. In *Mus*, this was first done in the medial extrastriolar region as a negative control for oncomodulin expression. After measuring the mean intensity of 100 medial extrastriolar hair cells, the minimum level of intensity was determined to be the mean of the distribution plus 3.7 times the standard deviation of the distribution. Any hair cell with a measured mean intensity above that of the minimum level of intensity was considered Ocm positive. This minimum level of intensity was determined individually for each specimen in order to accommodate any slight variations in fixation, immunohistochemical processing, or imaging parameters. With this metric, any hair cell with a mean level of intensity less than that of the determined minimum level of intensity was considered to have a 0.9999 probability being Ocm negative.

In *Rousettus*, if we used the same criterion as the mouse there were relatively high Ocm intensities in many if not most hair cells leading to the categorization of most hair cells as Ocm positive initially. This is evident when viewing a no primary control alongside the medial extrastriola of a positive specimen processed and imaged in parallel as most hair cells in the positive specimen exhibited a low level of Ocm expression (Figure 3). Unfortunately, we had to approach this problem a little differently in *Rousettus*. In order to determine a minimum level of intensity in the *Rousettus*, 100 mean intensity measurements were taken throughout the striola, using a uniform region of interest circle. These measurements were heavily skewed towards saturation, and the minimum level of intensity was determined to be the median minus 3.5 times the standard deviation of the distribution. Again, this was repeated for each specimen individually in order to accommodate any slight variations in fixation, immunohistochemical processing, or image parameters. With this metric, any hair cell with a mean level of expression

greater than that of the determined minimum level of intensity was considered to have a 0.9998 probability of being Ocm positive, allowing for the identification of those hair cells that exhibit a higher Ocm expression in the striola.

In addition to determining phenotypes of hair cells in the striola, the morphology of the afferents associated with type I hair cells was examined. Calyces in the striola were categorized as being simple or complex. Complex calyces receive input from more than one hair cell, whereas simple calyces encapsulate only one hair cell (Fernandez et al., 1990). We further restricted our description of complex calyces to a group of calyces arising from a single parent axon projecting onto multiple type I hair cells with shared calyceal walls between each hair cell. Complex calyces were further subdivided as doublet, triplets, quadruplets, quintuplets and sextuplets. This was done in *Neurolucida* using the channel representative of β3T labeling. The designation of calyces was determined by identifying the tops of calyces and visually following the top of the calyx to the base. Complex calyces were marked when more than one calyx top merged into a single base. Doublets were identified as two tops merging into one base and similar numbering scheme was adopted in order to identify triplets, quadruplets and so on.

Statistical analysis

Statistical analysis was done in R typically using bootstrap resampling methods. The general hypotheses that were tested were that the various distributions between *Rousettus* and *Mus* were similar. Since the hypothesis concerned the entire distributions of each species, it seemed appropriate to pool the data in order to perform a Monte Carlo resampling analysis. In order to verify the validity of pooling the data, the aggregate *Rousettus* distribution was compared to each individual specimen distribution to substantiate that the individual

distributions were not significantly different from the aggregate distribution. Examples of this verification are represented in Figure 1. The *Rousettus* hair cells were arranged in a 1411-element array (total number of striolar hair cells in *Rousettus*) where each element was assigned the characteristic of type I or type II hair cell according to the native aggregate distribution. 413 elements (the total number of hair cells in the striola of *Rousettus* specimen 1) were resampled with replacement, and the number of resampled type I and type II hair cells were summed and stored. This resampling was repeated 100,000 times and the histogram in Figure 1A shows the fraction of striolar type I hair cells (relative to total number of striolar hair cells) for the 100,000 resampled distributions. The red line indicates the position of the fraction of striolar type I hair cells (relative to total number of striolar hair cells) from the native *Rousettus* specimen 1 distribution relative to the resampled distributions. This entirety of this process was repeated for *Rousettus* specimens 2 and 3 (Figures 1B and 1C respectively) with 510 and 458 elements resampled from the aggregate distribution (total number of striolar hair cells from *Rousettus* specimens 2 and 3 respectively). For each comparison, it was determined that the individual specimen distribution was not significantly different from the aggregate distribution ($p=0.0585$, $p=0.618$, and $p=0.166$ for *Rousettus* specimens 1, 2 and 3 respectively).

Additionally in order to verify the validity of pooling the data for the Mus specimens, a similar process was repeated for the Mus specimens by resampling 431, 472, and 424 elements (total number of striolar hair cells from Mus specimens 1, 2, and 3 respectively) from a 1327-element aggregate array (total number of striolar hair cells in Mus). For each comparison, it was determined that the individual specimen distribution was not significantly different from the aggregate distribution ($p=0.268$, $p=0.222$, and $p=0.938$ for Mus specimens 1, 2 and 3 respectively).

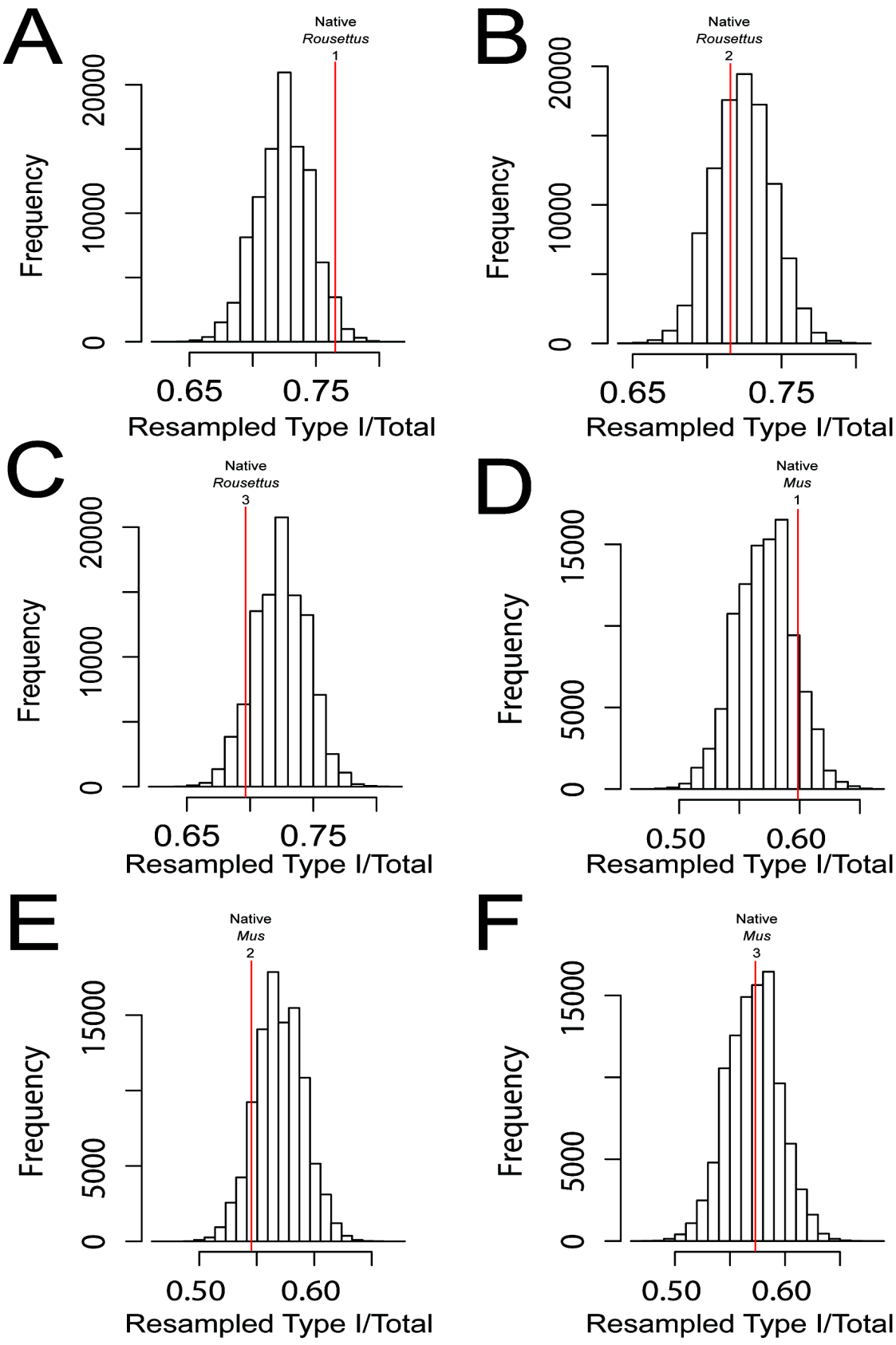
A
Native
Rousettus
1
Frequency
0
10000
20000
0.65
0.75
Resampled Type I/Total
B
Native
Rousettus
2
Frequency
0
10000
20000
0.65
0.75
Resampled Type I/Total
C
Native
Rousettus
3
Frequency
0
10000
20000
0.65
0.75
Resampled Type I/Total
D
Native
Mus
1
Frequency
0
5000
15000
0.50
0.60
Resampled Type I/Total
E
Native
Mus
2
Frequency
0
5000
15000
0.50
0.60
Resampled Type I/Total
F
Native
Mus
3
Frequency
0
5000
15000
0.50
0.60
Resampled Type I/Total

Figure 1. The fraction of striolar type I hair cells (relative to total number of striolar hair cells) for 100,000 distributions resampled from the native *Rousettus* aggregate distribution are shown in histograms for *Rousettus* specimens 1, 2 and 3 (A, B and C respectively), and the fraction of striolar type I hair cells (relative to total number of striolar hair cells) for 100,000 distributions resampled from the native *Mus* aggregate distribution are shown in histograms for *Mus* specimens 1, 2 and 3 (D, E and F respectively). Red lines indicate the native fraction of striolar type I hair cells (relative to total number of striolar hair cells) for each individual specimen relative to the resampled distributions. Each individual specimen distribution was not significantly different from the respective species aggregate distribution ($p=0.0585$, $p=0.618$, and $p=0.938$ for *Rousettus* specimens 1, 2 and 3 respectively and $p=0.268$, $p=0.222$, and $p=0.938$ for *Mus* specimens 1, 2 and 3 respectively).

When examining the hypotheses for *Rousettus* and *Mus* species comparisons, if an individual hypothesis was not supported then this led to the conclusion that the factors underlying production of the distributions were different. Significance was determined with an $\alpha=0.05$. These methods were developed in part as a reflection of those methods used in the Hoffman et al. Individual hypotheses were examined as follows.

For the comparison of striolar type I and type II hair cells, *Rousettus* hair cells were arranged in a 1411-element array where each element was assigned the characteristic of type I or type II hair cell according to the native distribution. 1327 elements were then resampled from this distribution with replacement. The number of resampled type I and type II hair cells were then summed and stored. This process was repeated 100,000 times and the native *Mus* fraction of type I and type II hair cells was compared to the 100,000 resampled type I and type II fractions.

When comparing the distribution type I_c and type I_d hair cells between each species, *Rousettus* hair cells were arranged in a 1411-element array where each element was assigned the characteristic of type I_c, type I_d, or type II hair cell. 1327 elements were then resampled from this distribution with replacement. The number of resampled type I_c, type I_d, or type II hair cells were summed and stored. This process was repeated 100,000 times and the fraction of type I_c and type I_d hair cells relative to total type I hair cells for each resampled distribution was compared to the native fraction of type I_c and type I_d hair cells relative to total type I hair cells in *Mus.*

In order to compare the expansion of Ocm into the extrastriola in *Rousettus* and *Mus*, *Rousettus* Ocm positive hair cells were arranged into a 1302-element array (the number of hair cells that were considered Ocm positive across the *Rousettus* utricles) where each element was assigned the characteristic of being striolar or extrastriolar. 917 elements (the number of Ocm positive hair cells across *Mus* utricles) were then resampled from this distribution with replacement. The number of extrastriolar and striolar hair cells for each resampled distribution were then summed and stored. This process was repeated 100,000 times and the fractions of extrastriolar Ocm positive and striolar Ocm positive hair cells (relative to all Ocm positive hair cell) for each resampled distribution was compared to the native fractions of extrastriolar and striolar Ocm positive hair cells in *Mus.*

To examine Ocm expression within the striola, *Rousettus* striolar hair cells were arranged into a 1411-element array where each element was assigned the characteristic of being Ocm positive or Ocm negative. 1327 elements were then resampled from this distribution with replacement. The number of Ocm positive and Ocm negative hair cells were summed and stored, and this process was repeated 100,000 times. The fractions of Ocm positive and Ocm negative hair cells relative to all striolar hair cells were compared between the resampled distributions and the native *Mus* distribution.

In examining the expression of Ocm in type I hair cell subtypes, *Rousettus* hair cells were arranged in a 1411-element array where each element was assigned the characteristic of type I_c, type I_d, or type II hair cell according to the native distribution. 1411 elements were then resampled from this distribution with replacement. The number of resampled type I_c, type I_d, and type II hair cells were then summed and stored, and this process was repeated 100,000 times. The native fraction of type I_c and type I_d Ocm positive hair cells relative to all type I Ocm positive

hair cells was compared to the fractions of type I_c and type I_d hair cells (relative to all type I hair cells) of the resampled distributions. Additionally, to compare the expression of Ocm in type I hair cell subtypes in *Rousettus* and *Mus* the a 1411-element array with characteristics of being Ocm+ type I_c, Ocm +type I_d, Ocm+ type II, Ocm- type I_c, Ocm- type I_d, or Ocm- type II was assigned to each hair cell according to the native distribution of *Rousettus* hair cells. This array was resampled with 1327 elements with replacement. The number of resampled Ocm+ type I_c, Ocm +type I_d, Ocm+ type II, Ocm- type I_c, Ocm- type I_d, and Ocm- type II hair cells were then summed and stored, and this process was repeated 100,000 times. The native fraction of Ocm+ type I_c and Ocm +type I_d hair cells (relative to all Ocm+ type I hair cells) in *Mus* was compared to the fractions of Ocm+ type I_c and Ocm +type I_d hair cells (relative to all Ocm+ type I hair cells) from the resampled distributions.

To examine the distributions of complex calyces in *Rousettus* and *Mus*, a 633-element array was created from the distribution *Rousettus* afferents projecting into the striola. Each element was assigned the characteristic of being a singlet, doublet, triplet, quadruplet, quintuplet, or sextuplet. 543 elements (total number of *Mus* afferents projecting into the striola) were then resampled from this distribution. The number of singlets, doublets, and triplets were then summed and stored. This was repeated 100,000 times. The fraction of singlets, doublets, and triplets, relative to all afferents from the resampled distributions were then compared to the native fractions of *Mus* singlets, doublets and triplets relative to all afferents.

RESULTS

Hair cell distribution

There is an increased fraction of striolar type I hair cells, relative to all striolar hair cells, in Rousettus aegyptiacus in comparison to Mus musculus.

In mammalian vestibular epithelia, there exists two hair cell types that are categorized based on the afferent ending upon which they project. Our principal finding was discovered while examining the distributions of type I (hair cells that project onto calyces) and type II (hair cells that project onto boutons) hair cells within the utricular striolae, of *Rousettus* and *Mus.* Low power maximum intensity projections of *Rousettus* and *Mus* utricles with outlines of the striola are represented in Figures 2A and 2B. Within the striola, each hair cell was identified as a type I or a type II. While type I hair cells were identified by the presence of a calyx (β3T, white), the type II hair cells were counted using a subtractive method. Phal, labels the stereocilia allowing for an accurate count of all hair cells within a region (i.e. the striola), and by subtracting the total number of type I hair cells from the total number of striolar hair cells, the total number of striolar type II hair cells was obtained. Figures 2C and 2D shows locations of striolar type II hair cells as indicated by magenta squares. The inset of Figure 2C displays the manner by which type II hair cells were located and labeled. The inset was created from a single optical section from a z-stack through a region of the striola. The phal labeling is represented in cyan while β3T immunolabeling is shown in white. In cyan, the base of the stereocilia and the kinocilium void can be visualized indicating the presence of a hair cell, while the white ring shows the apical portion of a calyx indicating that the hair cell at that location is surrounded by a calyx and is a type I hair cell. Hair cells identified without the presence of β3T were labeled as type II hair

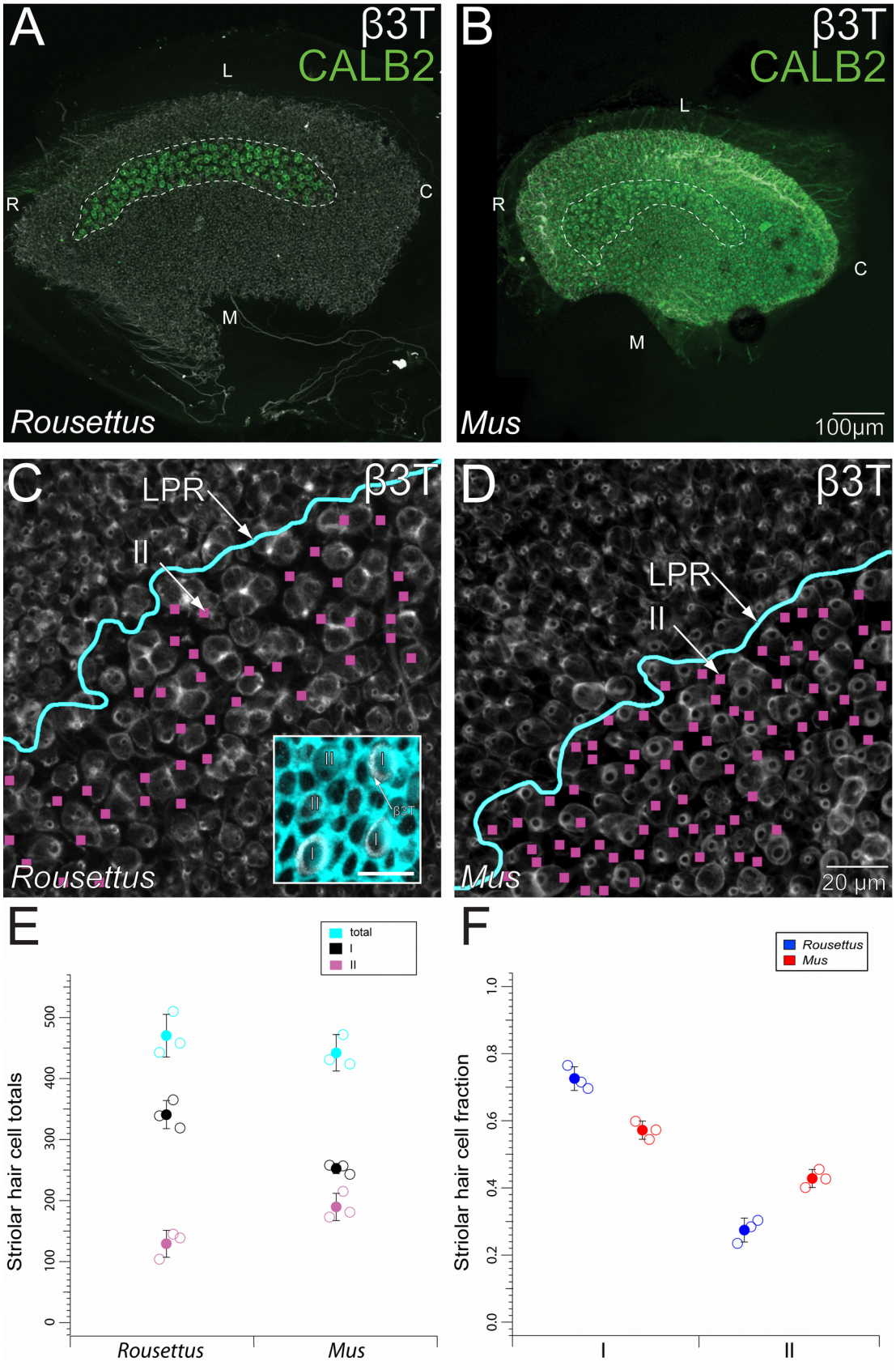
A
β3T
CALB2
L
R
C
M
Rousettus
B
β3T
CALB2
L
R
C
M
Mus
100µm
C
LPR
II
β3T
II
I
II
β3T
I
Rousettus
D
β3T
LPR
II
Mus
20 µm
E
total
I
II
Striolar hair cell totals
0
100
200
300
400
500
Rousettus
Mus
F
Rousettus
Mus
Striolar hair cell fraction
0.0
0.2
0.4
0.6
0.8
1.0
I
II

Figure 2. Low power average intensity projections of utricles from *Rousettus* (A) and *Mus* (B). Calretinin (Calb2, green) expressing calyces demarcate the striolae in both species (dashed line). β-3-tubulin (β3T, white) is expressed in all calyces and illustrates the relative size of the epithelia in comparison to the striola. In *Mus*, Calb2 is also expressed in hair cells. High power average intensity projections of the striola, which is medial to the line of polarity reversal (LPR, cyan), in *Rousettus* (C) and *Mus* (D). Type I hair cells are associated with immunolabeled calyces (β3T, white). The presence of all hair cells is indicated by positive stereocilia staining (C inset, Phal, cyan). Those hair cells not associated with a calyx (C inset, β3T, white rings) are determined to be type II hair cells (magenta squares). Inset scale bar represents 10 μm. The areas of imaged striolae are comparable, but there is an increased number of type II hair cells present in *Mus*. Total striolar hair cell counts in *Rousettus* and *Mus* are similar (E), but the relative fraction of type I to type II striolar hair cells varies significantly between *Rousettus* and *Mus* (F). Empty circles reflect counts from individual specimen while filled circles with bars represent the mean and standard deviation. Using resampling analysis, we tested the hypothesis that the relative fractions of type I and II hair cells (relative to total striolar hair cells) are similar in *Rousettus* and *Mus*. This analysis indicates that the fraction of striolar type I hair cells relative to total striolar hair cells is significantly greater in *Rousettus* than in *Mus* ($p < 10^{-5}$).

cells. Figures 2C and 2D illustrate that there appears to be fewer type II (magenta squares) hair cells in *Rousettus* (Figure 2C) when compared to *Mus* (Figure 2D) for similar regions of striolar epithelium suggesting a diminished density of type II hair cells in *Rousettus*.

Interestingly, despite the difference in size of the utricles, the total number of hair cells in the striolae of *Rousettus* and *Mus* were comparable (470 ± 35.1, 442 ± 25.9, respectively p= 0.334, Student's t-test) as shown in Figure 2E. We hypothesized that there would be similar fractions of type I hair cells relative to all striolar hair cells in *Rousettus* when compared to *Mus*. We attempted to recreate the *Mus* distribution of striolar hair cells by sampling the *Rousettus* distribution of striolar hair cells in order to simulate this hypothesis. The fraction of striolar type I hair cells relative to total striolar hair cells in *Rousettus* was significantly greater than in *Mus* (0.726 ± 0.0355 and 0.572 ± 0.0271 respectively, $p<10^{-5}$) as indicated in Figure 2F. These data indicate that the distribution of primary hair cell phenotypes is different in *Rousettus* when compared to *Mus*.

The fraction of type I_c and type I_d hair cells, relative to all type I hair cells, is comparable in <u>Rousettus aegyptiacus</u> and <u>Mus musculus</u>

After the principal finding of an increased fraction of type I hair cells relative to all

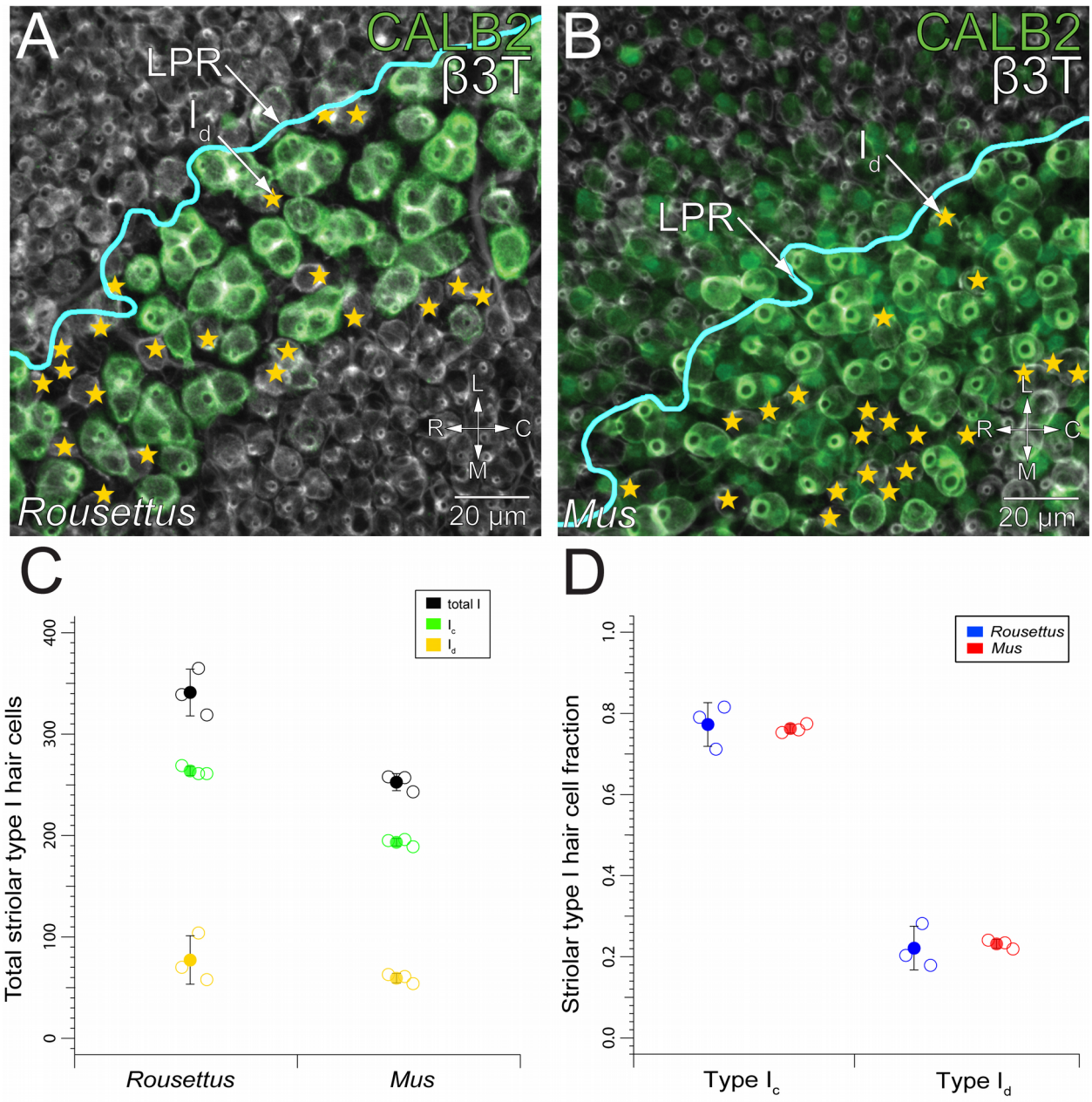

Figure 3. High power average intensity projections of the striola (medial to the LPR, cyan), in *Rousettus* (A) and *Mus* (B). Type I_c hair cells are associated with calyces that are co-localized for β-3-tubulin (β3T, white) and calretinin (Calb2, green). Type I_d hair cells (yellow stars) are associated with calyces that express β3T, but not Calb2. There are more striolar type I hair cells in *Rousettus* than in *Mus* (C), but fractions of type I_c and type I_d striolar hair cells (relative to total type I hair cells) are similar (D). Empty circles reflect counts from individual specimen while filled circles with bars represent the mean and standard deviation. Resampling analysis indicate that there is no significant difference between the relative distributions of type I_c and type I_d hair cells in the striola of *Rousettus* and *Mus* (p=0.584)

striolar hair cells in *Rousettus*, it was important to explore whether or not this expansion was related to either of the subtypes of striolar type I hair cell. Within the population of striolar type I

hair cells, the subtypes of type I_c and type I_d hair cells can be identified as those associated calretinin expressing calyces and those associated with non-calretinin expressing calyces respectively. High power average intensity projections of *Rousettus* and *Mus* striolae are shown in Figures 3A and 3B, and loci of type I_d hair cells are represented by Calb2-negative calyces (yellow stars), while type I_c hair cells can be identified as those associated with calyces co-localized for both Calb2 and β3T. The fraction of type I_c hair cells relative to total striolar type I hair cells was comparable in *Rousettus* and *Mus* (0.776 ± 0.0538 and 0.765 ± 0.0112 respectively, p=0.584, Figure 3C and 3D). In order to simulate the hypothesis that the fraction of type I_c hair cells relative to total striolar type I hair cells was comparable in *Rousettus* and *Mus*, we attempted to recreate the *Mus* type I subtype hair cell distribution from the *Rousettus* type I subtype distribution. While the total fraction of type I hair cells among all striolar hair cells was much greater in *Rousettus,* the relative distribution of subtypes (i.e. type I_c and type I_d) was comparable. This provided further evidence that the underlying factors responsible for the two phenotypes of type I hair cells are similar in *Rousettus* and *Mus*.

OCM expression

Regions of Ocm expression in <u>Rousettus aegyptiacus</u> and <u>Mus musculus</u> are comparable on a whole-tissue level, but differ upon closer inspection.

In 2010, Simmons et al, identified Ocm, a cytosolic calcium binding protein found in vestibular hair cells, as a striolar marker in mice and possibly other mammals. This finding was also substantiated by Hoffman et al. in a study revealing Ocm expression as restricted to the striolar and peristriolar regions of the utricle in *Mus*. Because of the relationship between Ocm

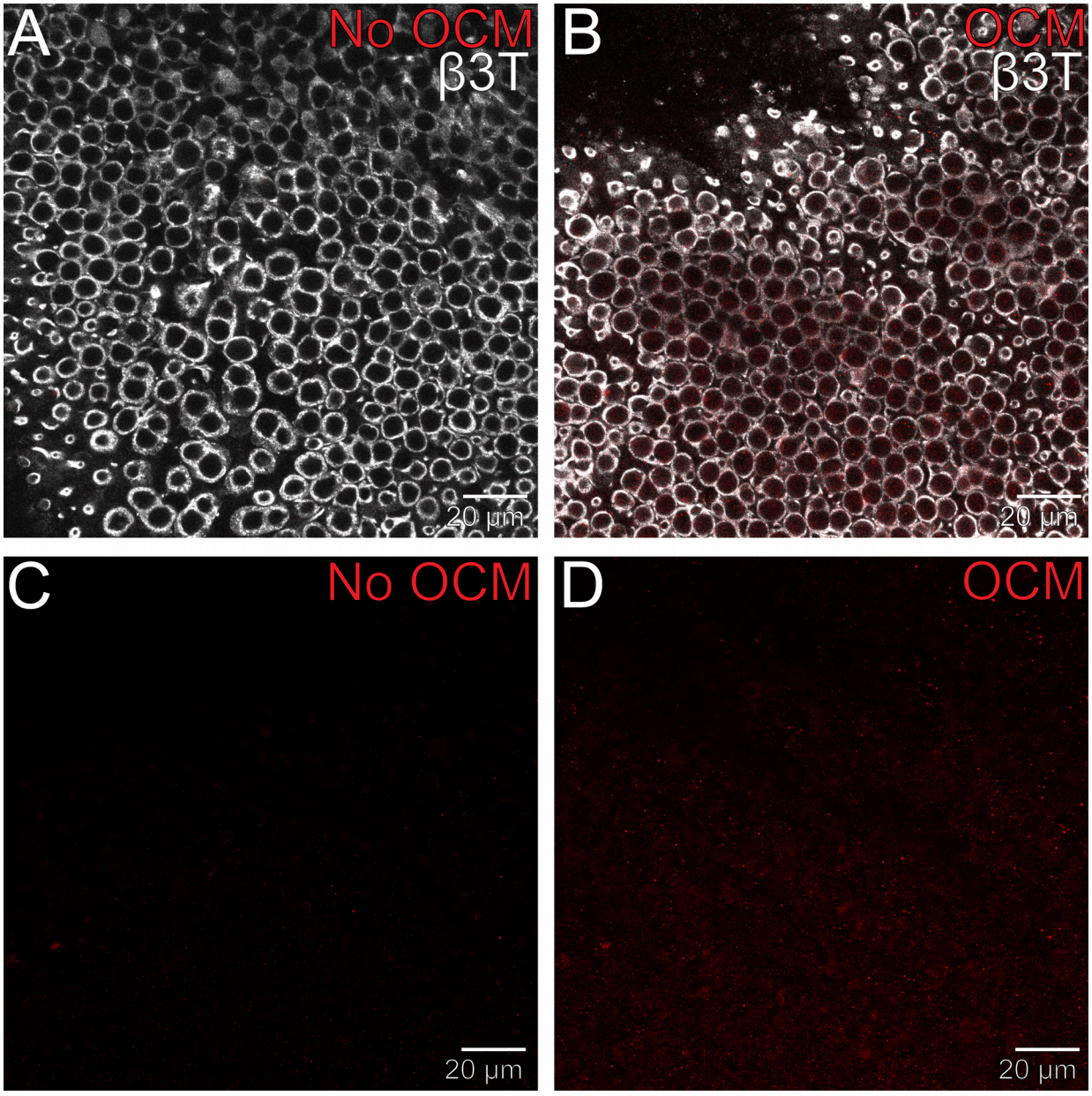

Figure 4. High power average intensity projections from *Rousettus*. The no primary control, with β3T overlayed and without (A, C, respectively), was imaged in the striola, a region where Oncomodulin (Ocm, red) expression was expected. The Ocm labeled specimen, with β3T overlayed and without (B, D, respectively), was imaged in the medial extra striola, where Ocm expression was not expected. There is a relatively high level of intensity in the medial extra striola of the Ocm labeled specimen when compared to the no primary control.

and the striola, it was hypothesized that there Ocm expression in the epithelia of *Rousettus* may be similar to Ocm expression in *Mus*. On a whole-tissue level the regions of expression in both *Rousettus* and *Mus* appeared to be similarly restricted to the striolar and peristriolar regions

(Figures 5A and 5B). However, upon closer inspection, there were quantifiable differences. As outlined in the *Methods*, in determining the minimum levels of intensity in each tissue it was revealed that *Rousettus* utricles exhibited some level of expression in most if not all hair cells when compared to the no-primary antibody control (Figure 4). Instead the quantification in *Rousettus* was limited to only identification of those hair cells that exhibit a higher Ocm expression in the striola.

Previous exploration into expression of Ocm in *Mus* found that the peristriolar expansion within *Mus* occurred to a great extent on the lateral border of the striola, lateral to the LPR (Hoffman et al.). Ocm hair cell counts from *Mus* as used in the present study were obtained from Hoffman et al. The open arrows in Figures 5C and 5D illustrate the expansion of Ocm expression into the medial and lateral peristriolar regions in *Rousettus* while the expansion of Ocm expression only extends into the lateral peristriolar region in *Mus*. Relative to the total population of Ocm+ hair cells, a greater fraction of hair cells were located in the extrastriola in *Rousettus* when compared to *Mus* (0.298 ± 0.0706 and 0.166 ± 0.0120 respectively, $p<10^{-5}$, Figures 5E). The hypothesis that the fraction of Ocm+ hair cells located in the extrastriola relative to all Ocm+ hair cells was similar in *Rousettus* and *Mus* was tested by attempting to recreate the *Mus* distribution of Ocm+ striolar and Ocm+ extrastriolar hair cells by resampling the *Rousettus* distribution of Ocm+ striolar and Ocm+ extrastriolar hair cells. Additionally, relative to all hair cells in the striola, there was a greater fraction of striolar Ocm+ hair cells in *Rousettus* than in *Mus (*0.641 ± 0.0453 and 0.577 ± 0.0245 respectively, $p=0.00672$, Figure 5F). Similarly, the hypothesis that the fraction of striolar Ocm+ hair cells was similar in *Rousettus* and *Mus* was tested by attempting to recreate the *Mus* distribution of Ocm+ striolar and Ocm- striolar hair cells by resampling the *Rousettus* distribution of all striolar hair cells. These findings indicate that the

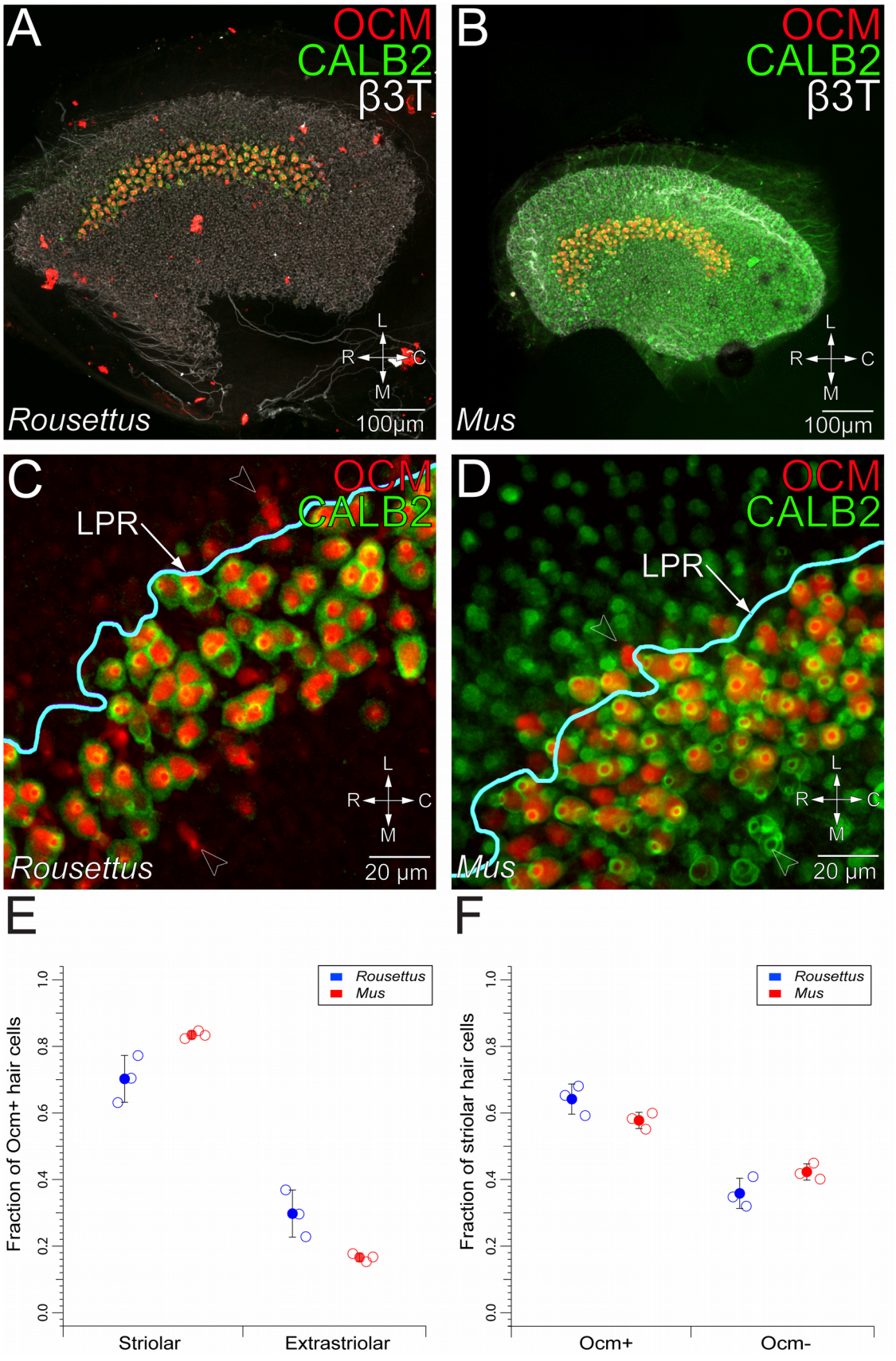
A
OCM
CALB2
β3T
L
R
C
M
Rousettus
100µm
B
OCM
CALB2
β3T
L
R
C
M
Mus
100µm
C
OCM
CALB2
LPR
L
R
C
M
Rousettus
20 µm
D
OCM
CALB2
LPR
L
R
C
M
Mus
20 µm
E
Rousettus
Mus
Fraction of Ocm+ hair cells
0.0
0.2
0.4
0.6
0.8
1.0
Striolar
Extrastriolar
F
Rousettus
Mus
Fraction of striolar hair cells
0.0
0.2
0.4
0.6
0.8
1.0
Ocm+
Ocm-

Figure 5. In *Rousettus* (A) and *Mus* (B), oncomodulin expression (Ocm, red) is restricted to the striolar and peristriolar regions in both species. Immunofluorescent labeling of calretinin (Calb2, green) in calyces demarcate the striola. Labeling for β-3-tubulin (β3T, white) illustrates the relative size of the epithelia in comparison to the striola. Ocm expression extends beyond the striola (medial to the LPR, cyan) in *Rousettus* (C) to a greater extent than *Mus* (D) as indicated by open arrows. Calb2 expressing calyces demarcate the striola. There are more Ocm expressing hair cells in *Rousettus* in *Mus* (not shown), but the relative fraction of extrastriolar Ocm+ hair cells (relative to all Ocm+ haircells) is greater in *Rousettus* than in *Mus*. ($p < 10^{-5}$, E). The fraction of striolar Ocm+ hair cells, relative to all striolar hair cells is greater in *Rousettus* and *Mus* ($p=0.00672$, F). Empty circles reflect counts from individual specimen while filled circles with bars represent the mean and standard deviation.

factors underlying Ocm expression in the striolar and peristriolar regions of the utricle *Rousettus* differ from those factors determining Ocm expression in *Mus*.

Expression of Ocm is non-random in striolar hair cell types and type I hair cell subtypes (i.e. type I vs. type II and. type I_c vs I_d) *in both Rousettus aegyptiacus and Mus musculus.*

In *Rousettus*, there were virtually no Ocm expressing type II hair cells in the striola (0.00484 ± 0.00566 relative to all Ocm+ striolar hair cells). Of the 865 Ocm+ striolar hair cells (i.e. among three specimens), only 4 were type II hair cells. In contrast, a substantial fraction of striolar Ocm expressing hair cells were type II hair cells (0.179 ± 0.0126) in *Mus*. Further analysis of Ocm expression in the striola was restricted to type I hair cells. The first question to address was whether or not Ocm expression was randomly distributed among type I hair cells (i.e. type I_c and I_d) or if there was some preference of Ocm expression among subtypes. In order to test this hypothesis, the fraction of Ocm+ type I_c hair cells relative to all Ocm+ type I hair cells in the striola was compared to the native fraction of type I_c hair cells relative to all type I hair cells in the striola. This was completed by attempting to recreate the striolar Ocm+ distributions of type I_c and type I_d hair cells by resampling from the native striolar distributions of type I_c and type I_d hair cells in both species. That is, if the number of type I_c Ocm+ hair cells were the result of random Ocm expression among all the striolar type I hair cells, it would be expected that the

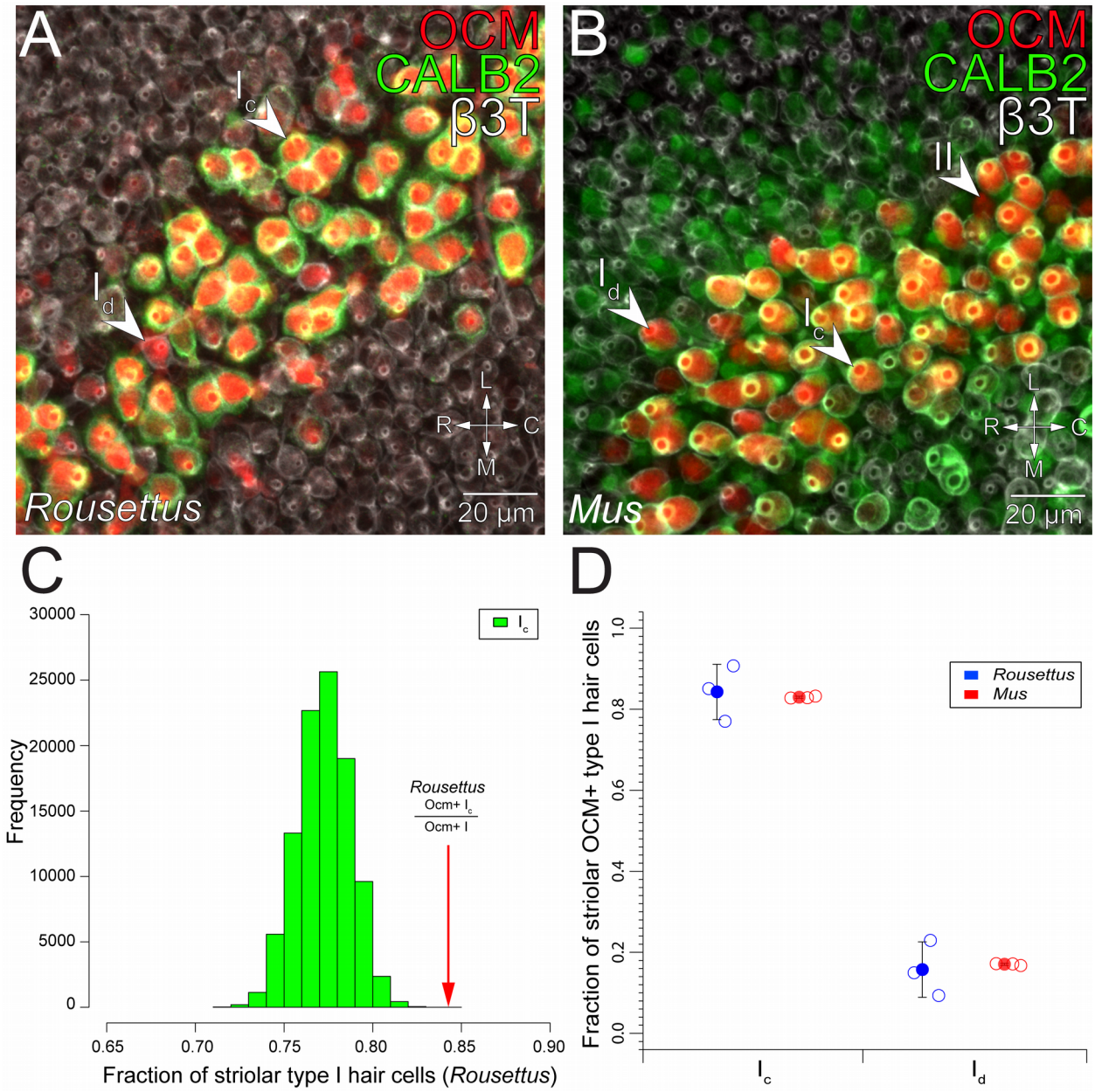

Figure 6. High power average intensity projections of the striola in *Rousettus* (A) and *Mus* (B). **There are almost no striolar oncomodulin (Ocm, red) expressing type II hair cells *Rousettus*.** Ocm expressing type I_c hair cells are associated with a calyx that is co-localized for calretinin (Calb2, green) and β-3-tubulin (β3T, white). Ocm expressing type I_d hair cells are associated with a calyx that is immunofluorescently labeled for only β3T. OCM expressing type II hair cells can be identified by lack of calyx. Arrows indicate examples of these phenotypes in *Rousettus* and *Mus*. We tested the hypothesis that Ocm expression in the striola is non-specific in type I hair cells. If Ocm expression was non-specific, the fraction of Ocm+ type Ic and striolar OCM+ type Id hair cells (relative to all striolar OCM+ type I hair cells) would be comparable to the native distribution of type I hair cells. In *Rousettus*, striolar OCM expression in type I hair cells is more closely associated with type I_c hair cells ($p < 10^{-5}$,C). This is consistent with Hoffman et al's findings in *Mus*. Fraction of Ocm+ type I_c hair cells relative to all Ocm+ type I hair cells is similar in *Rousettus* and *Mus* (p=0.432, D). Empty circles reflect counts from individual specimen while filled circles with bars represent the mean and standard deviation.

fraction of type I_c Ocm+ hair cells would be similar to the native distribution of type I_c hair cells

among all striolar type I hair cells. Both *Rousettus* and *Mus* showed increased Ocm expression in type I_c hair cells relative to all striolar Ocm+ type I hair cells when compared to their native distributions (0.843 ± 0.0684 compared to 0.776 ± 0.0538 in *Rousettus,* $p < 10^{-5}$, Figure 6C, and 0.830 ± 0.00256 compared to 0.765 ± 0.0112 in Mus, p=0.00004, Hoffman et al.). This finding indicates that in both *Rousettus* and *Mus*, Ocm expression is not randomly distributed among type I_c and type I_d hair cells.

Expanding upon the finding that Ocm expression amongst type I_c hair cells and I_d hair cells is non-random in both *Rousettus* and *Mus,* it was hypothesized that Ocm expression in type I_c and type I_d hair cells was similar in when comparing *Rousettus* and *Mus*. This hypothesis was tested by attempting to recreate the *Mus* distribution of striolar Ocm+ type I hair cells by resampling the *Rousettus* distribution of striolar Ocm+ type I hair cells. There was no increased preference for Ocm expression in type I_c hair cells in *Rousettus* in comparison to *Mus* (0.84263 ± 0.06847 and 0.82962 ± 0.00256 respectively, p=0.432, Figure 6D). Distribution of Ocm among type I hair cell subtypes was similar in *Rousettus* and *Mus* indicating that the factors governing this distribution is similar in both species. It should be noted that this is not true for striolar type II hair cells in *Rousettus*. It is evident that any factors underlying Ocm expression in *Rousettus* steers Ocm expression towards type I hair cells.

Simple vs complex calyces

There are fewer afferents ending in simple calyces projecting to the striola in Rousettus aegyptiacus than in Mus musculus.

Afferents with calyceal endings (both calyx only and dimorphic afferents, i.e. those

ending in both calyces and boutons) can be further categorized as being simple or complex. Those afferents ending in a single calyx, receiving input from one type I hair cell, were considered simple calyces, while those afferents ending in a compound calycx and receiving input from more than one type I hair cell were considered complex calyces (Fernandez et al., 1990). The complex calyces were further subdivided into doublets, triplets, quadruplets, quintuplets, and sextuplets based on the encapsulation of one, two, three, four, five, or six type I hair cells respectively. Examination of afferent differences in *Rousettus* and *Mus* were limited to singlets, doublets, and triplets because the number of quadruplets, quintuplets, or sextuplets in the striolae of both *Rousettus* and *Mus* specimens, as a fraction of total striolar afferents, was very small (0.0126 ± 0.00185, 0.00448 ± .00439, and 0.00156 ± 0.00270 respectively in *Rousettus*, 0.00357 ± 0.00617, 0, and 0 respectively in *Mus*). Additionally, the total number of afferents with quadruplet and higher complex calyces was not different in *Rousettus* when compared to *Mus* (4 ± 1.155 and 0.667 ± 1.732, respectively, p=0.0586, Student's t-test). We hypothesized that there would be no difference in the fractions of afferents with simple, doublet, and triplet endings relative to all afferents projecting from the striola. These hypotheses were tested by attempting to recreate the *Mus* distribution of calyx endings from the *Rousettus* distribution of calyx endings then comparing the bootstrapped distributions of fractions of simple, doublet, and triplet calyces to the native *Mus* fractions of simple, doublet and triplet calyces. For *Rousettus*, of the afferents projecting to the striola, a smaller fraction ended in simple calyces in *Rousettus* when compared to *Mus* (0.534 ± 0.0413 and 0.672 ± .0214, respectively, $p < 10^{-5}$). Conversely, of the afferents projecting to the striola, there was a greater fraction of afferents ending in doublets in *Rousettus* when compared to *Mus* (0.312 ± 0.0386 and 0.264 ± 0.0242, respectively, p=0.0206). Additionally, of the afferents projecting to the striola,

there was a greater fraction of afferents ending in triplets in *Rousettus* when compared to *Mus* (0.136 ± 0.0167 and 0.0608 ± 0.00915, respectively, $p < 10^{-5}$). These data indicate that Rousettus exhibits a greater fraction of calyx endings as complex calyces when compared to *Mus*.

KCNQ4 Expression

KCNQ4, a low-voltage activated K^+ channel expressed in adult vestibular calyces was briefly explored as another possible target for cellular adaptation. We conducted preliminary experiments to determine whether modifications in KCNQ4 expression could be detected in *Rousettus* utricles compared to the expression found in *Mus*. However, the antibody for KCNQ4 (*Neuromab*) used to label KCNQ4 in *Mus* specimens did not label KCNQ4 in *Rousettus.* With further investigation using the Uniprot Blast Tool to examine the peptide sequence of KCNQ4 it appears that the peptide for *Rousettus* KCNQ4 may be different than that of *Mus* as part of the cytosolic N-terminus that exists *Mus* KCNQ4 was truncated in *Rousettus* KCNQ4. This region of the truncated N-terminus contained the immunogen for KCNQ4 used in the *Neuromab* antibody. Using a different KCNQ4 antibody (SCBT), we were able to label *Rousettus* KCNQ4. Unfortunately, the use of two different antibodies may have unknown effects on labeling efficacy and therefore provided an obstacle in relation to performing a reliable quantitative analysis on the KCNQ4 specimen. On the basis of qualitative observation, both species exhibited heterogeneous KCNQ4 expression in calyces of the utricle with the high expression of KCNQ4 observed to be located in the striolar and peristriolar regions (Figures 7A and 7B). Additionally it seems that within the striola, there were some low KCNQ4 expressing calyces amongst the high

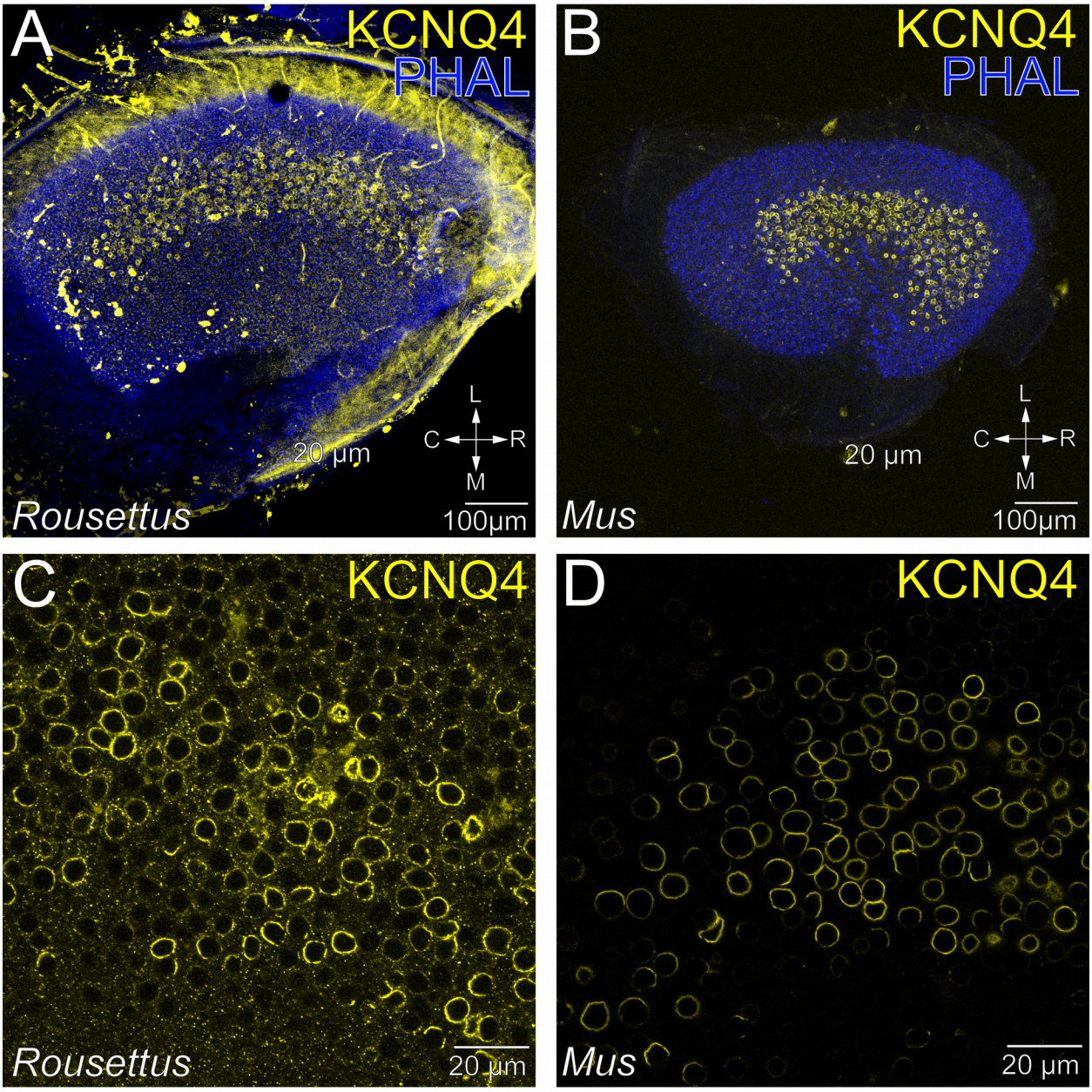

Figure 7. Low power average intensity projections of utricles from *Rousettus* (A) and *Mus* (B). Kv7.4 expression (KCNQ4, yellow) in calyces extends wells beyond the striola in both species. Fluorescently stained steriocilia (PHAL, blue) illustrates the relative size of the epithelia in comparison to the region of KCNQ4 expression. Although in the early stages of exploration, our preliminary findings suggest that KCNQ4 expression may also be expanded relative to the striola in *Rousettus* compared to *Mus*. Single optical sections in the striolar region of *Rousettus* (C) and *Mus* (D)

expressing calyces. Such qualitative observations were made by identifying KCNQ4 intensity levels visually as high or low. Areas of high levels of expression were compared to the striolae (as bounded by Calb2 expression calyces). Preliminary observation through high power stacks

indicated that the high levels of KCNQ4 expression may be expanded (i.e. extend further into the extrastriola) in *Rousettus* when compared to *Mus* (Figures 7C and 7D).

DISCUSSION

Adaptations for agile movement may present as increases in striolar type I hair cell density in Rousettus aegyptiacus.

The finding that there is an increased fraction of type I hair cells relative to all striolar hair cells in *Rousettus* when compared to *Mus* is indicative of a morphological adaptation in *Rousettus* that may have developed in response to evolutionary pressures for increased agility. Despite different methodologies used by Desai et al. (2005), their findings on the fractions of type I hair cells relative to all striolar hair cells in *Mus* were similar to the findings of the present study. Extending to Desai et al's (2005) findings that the fraction of striolar type I hair cells was similar in many terrestrial rodents, it is exceptional that there is a distinct and significant increase in the fraction of striolar type I hair cells in *Rousettus* in comparison to *Mus*. It is possible that these differences are reflective of adaptations to the need for increases in agility resultant of the flight and echolocation behaviors seen in *Rousettus*. However, despite increases in overall striolar type I hair cell fraction in *Rousettus*, the underlying factors for determining type I hair cell subtypes remains unchanged between *Rousettus* and *Mus*. This indicates that while adaptations in *Rousettus* may be linked to type I hair cells, they may not be linked to specific type I hair cell subtypes.

In Rousettus aegyptiacus when compared to Mus musculus, a larger fraction of striolar afferents with calyces terminate in complex calyces as opposed to simple calyces.

In *Rousettus*, we have seen that there is an increased fraction of type I hair cells in relative to all striolar hair cells when compared to *Mus*, and there is also a decline in the fraction of simple calyces. Desai et al. (2005) noted that the fraction of doublets and triplets was similar

across all the terrestrial rodents in their study. This was not true for in our comparison between *Rousettus* and *Mus*, as there was an increased fraction of both doublets and triplets in *Rousettus*. Taken together, these findings indicate that a large part of the expansion of type I hair cells in the *Rousettus* striola is accompanied by an increase in the complexity of the calyces upon which those hair cells project.

In Goldberg et al. (1990) it was noted that the most sensitive afferents projected to the striola. Additionally, following the logic presented in Fernandez et al. (1990), afferents receiving input from multiple hair cells of the same polarity may experience increased sensitivity to stereocilia deflection as the multiple inputs serve as signal amplification. In *Rousettus*, we see a greater proportion of highly sensitive afferents exhibiting this form of morphologic signal amplification.

The expansion of Ocm expression and a possible presynaptic mechanism for improved stimulus coding.

Rousettus shows some level of Ocm expression in the peripheral extrastriolar regions of the utricle. Even limiting our study to those hair cells that exhibit high Ocm expression, *Rousettus* tissues show distinct characteristics including little to no expression of Ocm in type II hair cells, increased expansion of expression into the peristriolar regions when compared to *Mus*, and overall increases in the fraction of striolar hair cells that express Ocm when compared to *Mus*. While the exact function of Ocm has yet to be elucidated, it is clear that Ocm expression in *Rousettus* is not only increased in the utricles, but tied more closely to type I hair cells. Despite the many differences in oncomodulin expression between *Rousettus* and *Mus*, the underlying

factors for determining oncomodulin expression in striolar type I hair cell subtypes remains unchanged. Taken with the earlier noted findings on type I and type II hair cells distributions in *Rousettus*, our findings suggest that adaptations to pressures requiring agile movement in *Rousettus* may be linked to type I hair cells, but not specifically type I hair cell subtypes.

Insight into the role of Ocm or β-parvalbumin may come from examining the functional role of another isoform, α-parvalbumin. A cytosolic calcium binding protein, α-parvalbumin is expressed in fast-spiking GABAergic interneurons in the mammalian central nervous system (Hu et al., 2014). α-parvalbumin acts as an antifacilitation factor by shunting local Ca^{2+} buffer concentration in the synaptic terminals (Eggermann and Jonas, 2012). Functionally, this may prevent continued neurotransmitter release from the presynaptic terminals resulting in shorter EPSPs. With shorter EPSPs, the postsynaptic terminal can repolarize more quickly, returning to a state in which it can respond to the next neurotransmitter release. If Ocm is functionally similar to α-parvalbumin, Ocm might perform a similar role in vestibular hair cells constituting a cellular mechanism associated with high frequency head movement coding. The distribution of Ocm expression in *Rousettus* suggests that *Rousettus* exhibits an adaptation for high frequency head movement coding observed through the expansion of Ocm in the striolar and peristriolar regions.

The expansion of KCNQ4 expression and a possible postsynaptic mechanism for improved stimulus coding

The function of KCNQ4 in the vestibular system has been explored by other investigators in recent years. They have also observed increased KCNQ4 expression in calyces in the striolar and peristriolar regions of the utricle in mice in addition to the analogous region of the central zone in the cristae of gerbils (Spitzmaul et al., 2013; Meredith and Rennie, 2015). KCNQ4

knockout mice exhibit vestibular dysfunction in the form of altered vestibulo-ocular reflex (Spitzmaul et al., 2013). Additionally, with the administration of KCNQ channel blockers, slow repolarization and decreased firing rate were observed in vestibular calyces in both central and peripheral zones (Meredith and Rennie, 2015). KCNQ channels are important for rapid repolarization of the postsynaptic membrane after neurotransmitter release by increasing outward K^+ current at low-voltages (Meredith and Rennie, 2015). KCNQ channels provide a postsynaptic mechanism serving to truncate EPSPs allowing the postsynaptic terminal to more readily respond to the next neurotransmitter release. Accomplishing the same goal, this is an alternative mechanism to the possible role of Ocm presynaptically. Meredith and Rennie's work also suggests that KCNQ4 has a greater contribution to outward K^+ currents in the central zone when compared to the peripheral zone. The increases in KCNQ4 expression in the *Rousettus* striolar and peristriolar regions suggests that *Rousettus* exhibits another adaptation resulting from expanded cellular mechanism consistent with improved coding ability for higher frequency stimuli. Because of the greater fraction of type I hair cells in *Rousettus*, the temporal coding advantage provided by KCNQ4 is more robustly expressed in *Rousettus* compared to *Mus*. Additionally, if we return to the finding that in *Rousettus* striolar Ocm expression is limited to type I hair cells, *Rousettus* exhibits adaptations for enhanced high frequency head movement coding resultant from expansion of possible presynaptic and postsynaptic mechanisms.

Future directions

It is our hope that the findings presented here will spur additional investigation into cellular adaptations in the vestibular system of *Rousettus*. For example, it is important to

examine whether or not the adaptations found in the utricle extend to other vestibular epithelia, such as the cristae. Additionally, recordings from vestibular afferents and recordings of natural head movement from *Rousettus* in flight would add physiological and behavioral context to our findings. While this study has provided novel evidence for cellular adaptations within the vestibular system in *Rousettus,* there is still much exploration to be done in order to elucidate the true extent and functional role of these adaptations.

REFERENCES

Beraneck M, Cullen KE (2007) Activity of vestibular nuclei neurons during vestibular and optokinetic stimulation in the alert mouse. Journal of Neurophysiology 98:1549-1565.

Davies KT, Bates PJ, Maryanto I, Cotton JA, Rossiter SJ (2013) The evolution of bat vestibular systems in the face of potential antagonistic selection pressures for flight and echolocation. PloS One 8:e61998.

Desai SS, Zeh C, Lysakowski A (2005) Comparative morphology of rodent vestibular periphery. I. Saccular and utricular maculae. Journal of Neurophysiology 93:251-266.

Eggermann E, Jonas P (2012) How the 'slow' Ca(2+) buffer parvalbumin affects transmitter release in nanodomain-coupling regimes. Nature Neuroscience 15:20-22.

Fernandez C, Goldberg JM, Baird RA (1990) The vestibular nerve of the chinchilla. III. Peripheral innervation patterns in the utricular macula. Journal of Neurophysiology 63:767-780.

Goldberg JM, Desmadryl G, Baird RA, Fernandez C (1990) The vestibular nerve of the chinchilla. V. Relation between afferent discharge properties and peripheral innervation patterns in the utricular macula. Journal of Neurophysiology 63:791-804.

Hoffman LF, Choy KR, Sultemeier DR, Simmons DD (Submitted) Oncomodulin expression reveals new insights into the cellular organization of the murine utricle striola.

Horowitz SS, Cheney CA, Simmons JA (2004) Interaction of vestibular, echolocation, and visual modalities guiding flight by the big brown bat, Eptesicus fuscus. Journal of Vestibular Research: Equilibrium & Orientation 14:17-32.

Hu H, Gan J, Jonas P (2014) Interneurons. Fast-spiking, parvalbumin(+) GABAergic interneurons: from cellular design to microcircuit function. Science 345:1255263.

Lasker DM, Han GC, Park HJ, Minor LB (2008) Rotational responses of vestibular-nerve afferents innervating the semicircular canals in the C57BL/6 mouse. Journal of the Association for Research in Otolaryngology 9:334-348.

Lettvin JY, Maturana HR, McCulloch WS, Pitts WH (1959) What the frog's eye tells the frog's Brain. Proceedings of the Institute Radio Engineers 47:1940-1951.

Liu Y, Han N, Franchini LF, Xu H, Pisciottano F, Elgoyhen AB, Rajan KE, Zhang S (2012) The voltage-gated potassium channel subfamily KQT member 4 (KCNQ4) displays parallel evolution in echolocating bats. Molecular Biology and Evolution 29:1441-1450.

Lysakowski A, Gaboyard-Niay S, Calin-Jageman I, Chatlani S, Price SD, Eatock RA (2011) Molecular microdomains in a sensory terminal, the vestibular calyx ending. The Journal of Neuroscience 31:10101-10114.

Meredith FL, Rennie KJ (2015) Zonal variations in K+ currents in vestibular crista calyx terminals. Journal of Neurophysiology 113:264-276.

Potier S, Bonadonna F, Kelber A, Martin GR, Isard PF, Dulaurent T, Duriez O (2016) Visual abilities in two raptors with different ecology. The Journal of Experimental Biology.

Ramprashad F, Landolt JP, Money KE, Laufer J (1980) Neuromorphometric features and dimensional analysis of the vestibular end organ in the little brown bat (Myotis lucifugus). The Journal of Comparative Neurology 192:883-902.

Riskin DK, Iriarte-Diaz J, Middleton KM, Breuer KS, Swartz SM (2010) The effect of body size

on the wing movements of pteropodid bats, with insights into thrust and lift production. The Journal of Experimental Biology 213:4110-4122.

Si X, Zakir MM, Dickman JD (2003) Afferent innervation of the utricular macula in pigeons. Journal of Neurophysiology 89:1660-1677.

Simmons DD, Tong B, Schrader AD, Hornak AJ (2010) Oncomodulin identifies different hair cell types in the mammalian inner ear. The Journal of Comparative Neurology 518:3785-3802.

Spitzmaul G, Tolosa L, Winkelman BH, Heidenreich M, Frens MA, Chabbert C, de Zeeuw CI, Jentsch TJ (2013) Vestibular role of KCNQ4 and KCNQ5 K+ channels revealed by mouse models. The Journal of Biological Chemistry 288:9334-9344.

Steen JB, Mohus I, Kvesetberg T, Walloe L (1996) Olfaction in bird dogs during hunting. Acta Physiologica Scandinavica 157:115-119.

Ulanovsky N, Moss CF (2008) What the bat's voice tells the bat's brain. Proceedings of the National Academy of Sciences of the United States of America 105:8491-8498.